Origin of Anisotropic Photoluminescence in Heteroatom-Doped Carbon Nanodots

Jing, P.; Han, D.; Li, D.; Zhou, D.; Zhang, L.; Zhang, H.; Shen, D.; Qu, S.

DOI
10.1002/adom.201601049

Publication date
2017

Document Version
Final published version

Published in
Advanced Optical Materials

Origin of Anisotropic Photoluminescence in Heteroatom-Doped Carbon Nanodots

Pengtao Jing, Dong Han, Di Li, Ding Zhou, Ligong Zhang, Hong Zhang, Dezhen Shen, and Songnan Qu**

Because of the origin of anisotropic photoluminescence (PL) in carbon nanodots (CDots) is unclear, which greatly hampers precisely controlling their luminescence properties and relevant applications. Here, the anisotropic PL in heteroatom-doped CDots using polarization-dependent femtosecond transient absorption spectroscopy and computational simulation is studied. Anisotropic absorption and stimulated emission of CDots are observed in different solvents. Solvent effect on solvation relaxation is observed for CDots in different solvents, reflecting the dipole–dipole interaction between CDots and polar solvent molecules. Depolarization process is observed not only dependent on solvent viscosity but also related to the proton donation capability of solvent. The experimental and computational results reveal the anisotropic PL of CDots originate from neither intrinsic nor extrinsic states, but originates from n–π^* transition of a hybrid state, in which the highest occupied molecular orbital is localized at dopant atoms, such as pyridinic N and carbonyl O, and the lowest unoccupied molecular orbital is delocalized over graphene-like domain.

1. Introduction

Carbon nanodots (CDots), as an emerging new luminescent nanomaterials with sizes less than 10 nm, have been attracting much attentions and demonstrating a great potential application in bioimaging,[1–5] photocatalysis,[6–10] photovoltaics,[11–13] light emitting diodes,[14,15] and lasing materials,[16,17] due to their distinct merits, such as biocompatibility, bright fluorescence, high photostability, and low cost.[18–23] Recently, anisotropic photoluminescence (PL) of single CDot was proved to come from electric dipole via the scanning of azimuthally polarized laser beam (APLB) at focal region.[24] Inorganic semiconductor quantum dots (QDs), such as CdSe/ZnS QDs, show isotropic emission property under excitation of APLB.[25] Usually, the colloidal semiconductor quantum rods displayed linearly polarized emission, due to their dielectric contrast and asymmetric shape.[26,27] Super-resolution by polarization demodulation (SPoD) and excitation polarization angle narrowing (ExPAN) are newly developed super-resolution techniques,[28] usually based on organic fluorescent chromophore with a transition dipole moment. CDots show a potential application in polarization modulation based super-resolution microscopy. Additionally, linearly polarized luminescent CDots are also highly desirable in applications of lasing materials and polarized light-emitting diodes. However, origin of the PL, particularly of the anisotropic PL in CDots is unclear, which greatly hampers precisely controlling their luminescence properties and relevant applications. When addressing this issue properly, it should be noted that strong luminescence has always been observed in CDots with heteroatoms (such as N, O, or S) doping,[17,29–31] which makes the dopants under suspicion of contributing to transition dipole moment and lead to anisotropic PL. Thus, it is of great scientific interest to investigate the origin of the anisotropic PL in heteroatom-doped CDots.

The time-resolved spectroscopy is usually performed to understand the ultrafast dynamics of carrier relaxation and recombination in materials. Recently, ultrafast emission and carrier dynamics of CDots were studied by using femtosecond up-conversion technique and transient absorption (TA) spectroscopy under magic angle condition to avoid anisotropic effect.[32–34] Wen et al. suggested the emission of CDots consists of intrinsic and extrinsic states, respectively, from the sp^2 C conjugated domains and surface states.[32] Wang et al. attributed the origin of green luminescence in CDots and graphene quantum dots (GQDs) to the special edge states.[33,34] The main contribution for PL in CDots was considered to come from surface states with long decay lifetime, namely, so-called extrinsic states, molecule-like states, or special edge states. Nonetheless, the anisotropic PL origin of CDots remains under debate. The solvation and depolarization relaxation of CDots in various solvents were studied by time-correlated single photon counting

Dr. P. Jing, Dr. D. Han, Dr. D. Li, Dr. D. Zhou, Prof. L. Zhang, Prof. D. Shen, Prof. S. Qu
State Key Laboratory of Luminescence and Applications
Changchun Institute of Optics Fine Mechanics and Physics
Chinese Academy of Sciences
3888 Eastern South Lake Road, Changchun 130033, China
E-mail: qusn@ciomp.ac.cn
Dr. P. Jing, Prof. H. Zhang
Van't Hoff Institute for Molecular Sciences
University of Amsterdam
Science Park 904, Amsterdam 1098 XH, The Netherlands
E-mail: h.zhang@uva.nl

DOI: 10.1002/adom.201601049

(TCSPC) method with sub-nanosecond time resolution.[35–38] However, timescale of dipole–dipole interaction and depolarization is usually from tens of femtoseconds to tens of picoseconds. To the best of our knowledge, ultrafast anisotropy relaxation of CDots in femtosecond scale has not been investigated. It might be a breakthrough to reveal their anisotropic PL mechanism to well understand their PL origin through investigating the polarization-dependent ultrafast dynamic processes of CDots.

In this work, the ultrafast solvation and depolarization dynamics of heteroatom-doped CDots in various solvents were studied by polarization-dependent femtosecond TA spectroscopy. Anisotropic absorption and stimulated emission of CDots were observed in different solvents. Solvent effect on solvation relaxation was observed for CDots in different solvents, reflecting the dipole–dipole interaction between CDots and polar solvent molecules. Depolarization process was observed not only dependent on solvent viscosity but also related on the proton donation capability of solvent. The experimental and computational results reveal the anisotropic PL of CDots originates from neither intrinsic nor extrinsic states, but originates from n–π^* transition of a hybrid state, in which the highest occupied molecular orbital (HOMO) is localized at dopant atoms (such as pyridinic N and carbonyl O) and the lowest unoccupied molecular orbital (LUMO) is delocalized over graphene-like domain. These results are beneficial for well understanding the origin of the anisotropic PL from CDots.

2. Results and Discussion

The heteroatom-doped CDots were synthesized following a microwave-assisted bottom-up method from citric acid ($C_6H_8O_7$) and urea (CH_4N_2O), reported in our previous work.[17] The morphologies of CDots were characterized using transmission electron microscopy (TEM). The average size of CDots is 2.1 ± 0.5 nm (Figure S1a, Supporting Information). The high-resolution TEM (HR-TEM) image shows CDots have clear lattice fringes with an interplanar spacing of 0.21 nm (Figure S1b, Supporting Information), which is close to the (100) facet of graphitic carbon. The chemical composition of CDots was investigated by X-ray photoelectron spectroscopy (XPS) spectrum (Figure S2, Supporting Information). It is shown three peaks at 285, 400, and 531 eV, respectively, for C 1s, N 1s, and O 1s.[17,29] The high-resolution C 1s XPS spectrum shows five peaks at 284.5, 285.2, 285.7, 287.2, and 288.5 eV, respectively, for sp^2 C, sp^3 C, C—N, C—O, and C=O/C=N. Two peaks at 399.6 and 400.4 eV are observed in the high-resolution N 1s XPS spectrum, which are attributed to pyridinic N (C—N—C) and graphite N (N–(C)3). The high-resolution O 1s XPS spectrum shows two peaks at 530.9 and 531.6 eV, respectively, for quinone O and carbonyl O (C=O). The G band of CDot in the Raman spectrum was observed at 1578 cm^{-1}, as seen in Figure S3 (Supporting Information). The UV–vis spectrum of CDots (**Figure 1**a) has five absorption peaks at 225, 250, 275, 330, and 410 nm, respectively, corresponding to five optical transitions in CDots. Two strong excitation bands of the green emission of CDots were observed at 410 and 275 nm in fluorescence excitation-emission map (Figure 1b), corresponding to two optical

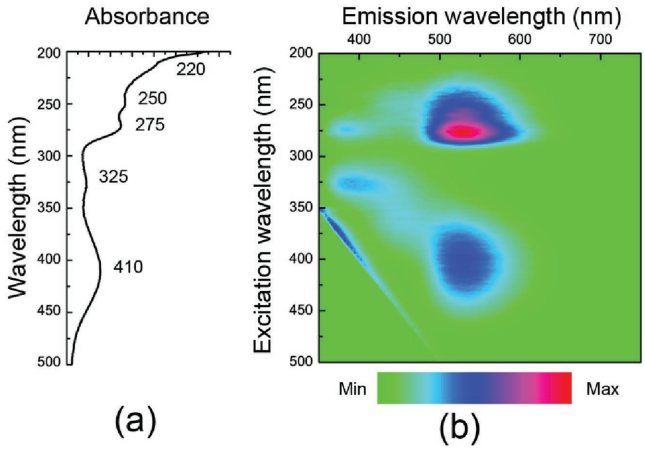

Figure 1. a) Static absorption spectrum and b) 3D fluorescence excitation-emission map of CDots in aqueous solution.

transitions from the ground state to the lowest excited state, and to higher excited state, respectively.

First, the femtosecond TA spectroscopic measurement of CDots in water under magic angle condition was carried out, as shown in **Figure 2**a. Upon femtosecond pulse excitation, a number of electrons in ground state are pumped into excited states resulting in the ground-state bleaching (GSB) feature at about 410 nm in TA spectrum (Figure 2b). Here three possible depopulation channels for electrons in excited states are spontaneous emission, stimulated emission (SE), and excited-state absorption (ESA), respectively. In general, spontaneous emission cannot be detected in TA spectrum. The SE process induced a negative feature at around 550 nm in TA spectrum (Figure 2b), meaning that more photons were generated subjected to probe pulse passing through the excited sample. Electrons in the lowest excited states can further absorb probe photons to jump to higher energy levels. Two ESA features were observed at 470 and 750 nm in Figure 2b. The decay time constant at 470 nm extends to nanosecond scale, which is similar to that of SE feature (Figure S4, Supporting Information). The decay time constant at 750 nm is only 0.5 ps, which is close to the fast decay component observed at 425 nm for GSB. The total energy of 3.0 eV (410 nm) and 1.7 eV (750 nm) or 2.3 eV (550 nm) and 2.6 eV (470 nm) is about 4.7–4.9 eV, which is close to the photon energy of optical transitions at around 4.5–5.0 eV (250–275 nm) (Figure 1a).

If the transition dipole moment exists in nanoparticle, dipole–dipole interaction between nanoparticles and polar solvent molecules should be considered in analysis of TA spectra. After excitation of polarized ultrashort laser pulse, charge distribution in nanoparticle changed. Then the polar solvent molecules would then subsequently reorient rapidly to reduce the system energy which could induce redshift of emission peak in time-resolved spectroscopy, so-called solvation relaxation (inset of Figure 2d).[39] A redshift of SE feature is clearly seen from the top-view TA data (Figure 2a), traced with a black solid line. TA kinetic traces of CDots in water probed at different wavelengths demonstrate the temporal evolution of SE process (Figure 2c). This phenomenon was widely observed in polar solution of dye molecules.[39,41] The time-dependent

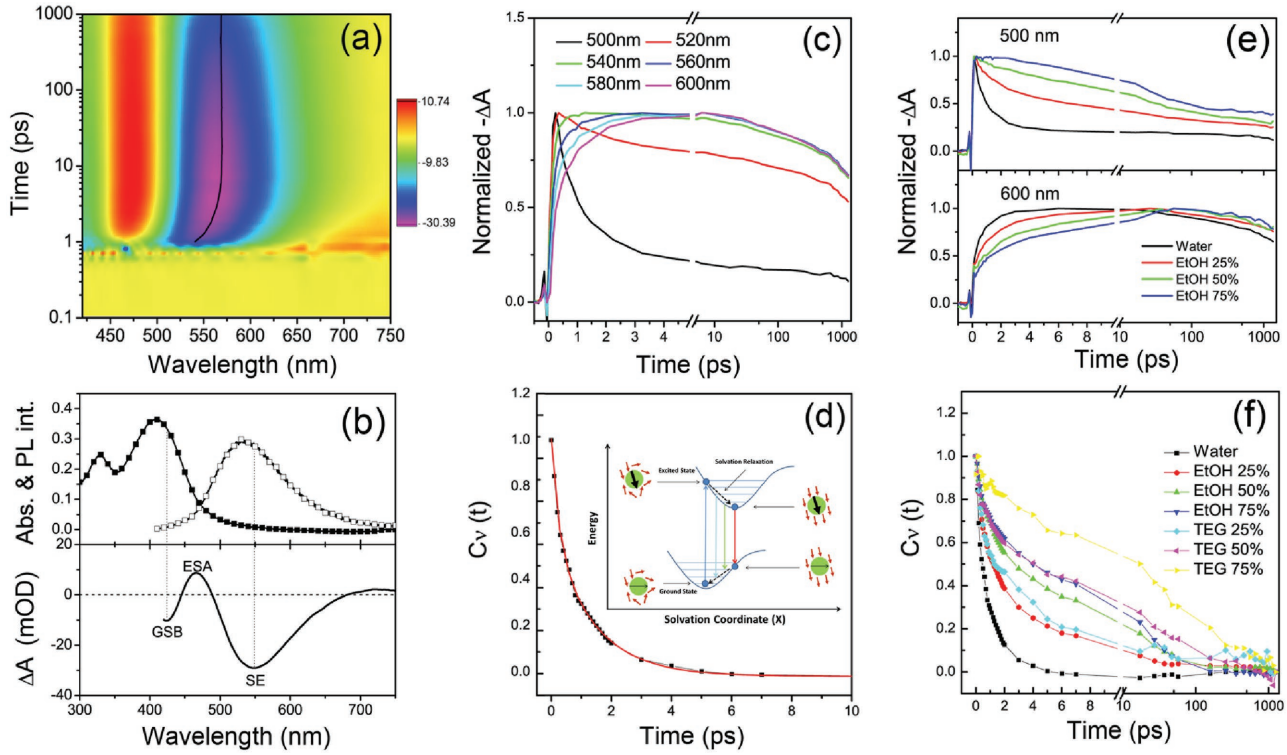

Figure 2. a) Top-view TA data (magic angle) of CDots in water. The black solid line shows the shift of SE peak. b) Static absorption (black solid squares), PL (black empty squares), and TA spectra delayed 1 ps after pump pulse (black solid line) of CDots in water. c) TA kinetic traces of CDots in water probed at different wavelengths ranging from 500 to 600 nm. d) The correlation function plotted as a function of time for CDots in water. Inset: A schematic illustration of solvation dynamics. Arrows represent the directions of dipoles. e) TA kinetic traces of CDots probed at 500 and 600 nm, dispersed in water and ethanol (25%, 50%, and 75%) aqueous solutions. f) The correlation functions plotted as a function of time for CDots in different solvents.

Stocks shift is usually described as the correlation function $C_v(t)$, defined as[39,40]

$$C_v(t) = \frac{\nu(t) - \nu(\infty)}{\nu(0) - \nu(\infty)} \quad (1)$$

where $\nu(0)$, $\nu(t)$, and $\nu(\infty)$ are the optical frequencies corresponding to the maxima of SE features in TA data at time zero, at time t, and at infinite time. The obtained decay time constants from a biexponential decay function are 0.23 ps (37%) and 1.29 ps (63%), respectively. The average solvation relaxation time for water is 0.90 ps, which is close to the reported values.[41,42] The excitation wavelength dependent emission of CDots was attributed to the slow solvation process (close to radiative decay lifetime, ≈ns).[35–37] The PL decays of CNDs in water from 500 to 600 nm show similar trend in Figure S5 (Supporting Information), indicating the slow solvation relaxation process in nanosecond scale is not observed in our experiment. It is predicted that the solvation relaxation process is slower in solution of higher viscosity (η), because it will experience stronger frictional interactions.[40] We varied the viscosities of solvents from 1.0 to 20.0 cP by tuning concentrations (%, v/v) of ethanol (EtOH) or triethylene glycol (TEG) in aqueous solution. Detailed properties of CDots in different solutions are given in Figures S6 and S7 (Supporting Information). Femtosecond TA measurements were performed to confirm the solvent effect on solvation relaxation process. The decay and rise processes in TA kinetic traces at 500 and 600 nm slow down with increasing the concentration of ethanol in aqueous solutions (Figure 2e). The correlation functions for CDots in water, ethanol, and TEG aqueous solutions (Figure 2f) were fitted by a biexponential decay function (Table S1, Supporting Information). The average solvation relaxation time is 12.34 ps for CDots in 75% ethanol aqueous solution (η: 1.9 cP), which is larger than that (3.05 ps) in 25% TEG aqueous solution (η: 2.7 cP). It should be noted that the solvation relaxation time is dependent on not only solution viscosity but also water volume fraction. The microscopic mechanism of solvation relaxation process is rapid reorientation of solvent molecules around CDot in the first shell.[40] Viscosity of solution represents interaction between solvent molecules. Higher viscosity slows down the rotation of solvent molecules. On the other hand, because volume of water molecule is smaller than that of ethanol or TEG molecule, water molecules are rotating faster than other solvent molecules in mixed solutions. Therefore, the solvation relaxation could slow down with increasing solution viscosity or decreasing water concentration. Time-dependent redshift of SE feature of CDots in different solvents could be attributed to the dynamic equilibrium of dipole–dipole interactions between CDots and solvent molecules, ensuring that the PL of CDots indeed comes from a dipole emission center.

We further investigated the ultrafast anisotropic relaxation of CDots in water by using TA spectroscopy under parallel and perpendicular polarization configurations (**Figure 3**a,b).

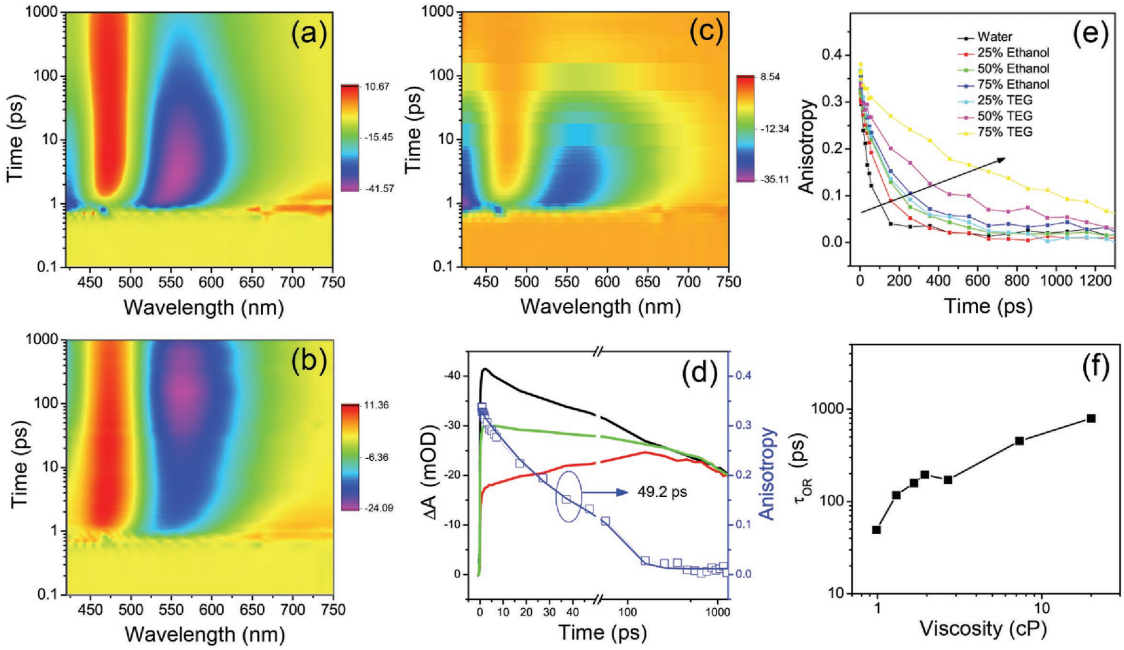

Figure 3. Top-view TA spectra of CDots in water, when polarizations of pump and probe were set to a) parallel and b) perpendicular. c) The difference spectrum between parallel and perpendicular TA spectra, $\Delta A_{||}(t) - \Delta A_{\perp}(t)$. d) TA kinetic traces of CDots probed at 550 nm. (Black, red, and green lines represent the parallel, perpendicular, and magic angle polarizations. Blue line is the calculated anisotropy as a function of delay time.) e) Time-dependent polarization anisotropy of CDots in different solvents. f) Reorientation times for CDots versus viscosity of solvents.

At time zero, the difference of TA signals between parallel and perpendicular polarization configurations is the largest. Afterward, CDots with dipole moments are randomly rotating until reaching an isotropic distribution. Two anisotropic features were observed for GSB band (420–450 nm) and SE band (490–650 nm) (Figure 3c). Besides, two isotropic features for positive ESA bands at 470 and 750 nm were also observed in the time range of 2–1000 ps and this phenomenon was solvent independent (Figure S8, Supporting Information). In literature, the isotropic carrier distribution in graphene was observed after delay time of 150 fs and the fast depolarization process is ascribed to carrier–phonon scattering.[43] Similarly, the isotropic ESA features of our CDots with delay time of 10 ps can be explained by fast depolarization process of carrier in π^* orbital (Figure S9, Supporting Information), which may be related to graphene-like structure in CDots.

To analyze orientational relaxation of CDots in solution, the time-dependent anisotropy is defined as[44]

$$R(t) = \frac{\Delta A_{||}(t) - \Delta A_{\perp}(t)}{\Delta A_{||}(t) + 2 \times \Delta A_{\perp}(t)} \tag{2}$$

where $\Delta A_{||}(t)$ and $\Delta A_{\perp}(t)$ are the transient absorption signal intensities under parallel and perpendicular configurations at delay time of t. The time-dependent anisotropy of SE was estimated from the TA kinetic traces at 550 nm of CDots under different polarization configurations (Figure 3d). The fitted orientational relaxation time constant (τ_{OR}) is 49.2 ps for CDots in water. Figure 3e shows the time-dependent anisotropy of stimulated emission for CDots in solutions with different viscosities. The initial anisotropies of CDots in different solutions are ranged from 0.35 to 0.39, which is close to the theoretical maximum (0.4) of anisotropy for a randomly oriented sample.[44] The depolarization time constants of CDots are enhanced from 49.2 to 793.5 ps with increasing the viscosity of solvent (Figure 3f). Generally, the random rotation of nanoparticles in solution is related with the interaction between solute and solvent, and described by the Debye–Stokes–Einstein (DSE) equation[40]

$$\tau_{OR} = \frac{\eta V}{k_B T} \tag{3}$$

where τ_{OR} is the orientational relaxation time constant, η is the bulk viscosity of the surrounding medium, V is the hydrodynamic volume, k_B is the Boltzmann constant, and T is the temperature. In our experiment, the calculated diameters of CDots in various solvents are about 0.7–0.9 nm from DSE equation, which is much smaller than the actual size of CDots (2.1 ± 0.5 nm). This phenomenon implies the depolarization of CDots in solution cannot be completely ascribed to the random rotation of the whole nanoparticle. It was reported that the magnitude and orientation of dipole moment in 3-hydroxyflavone derivatives showed large difference before and after proton transfer.[45] We propose that proton transfer could happen between water molecules and CDots, which might contribute to the faster depolarization process of CDots in aqueous solution.

In order to verify our hypothesis, we selected a polar aprotic solvent with similar viscosity to that of water for comparison. *N*,*N*-Dimethylformamide (DMF) is a typical polar aprotic solvent with viscosity of 0.9 cP at 20 °C, which is close to that of water (1.0 cP, 20 °C). Stokes shifts of CDots in water and DMF are 5596 and 3659 cm^{-1}, respectively (**Figure 4**a). It was also

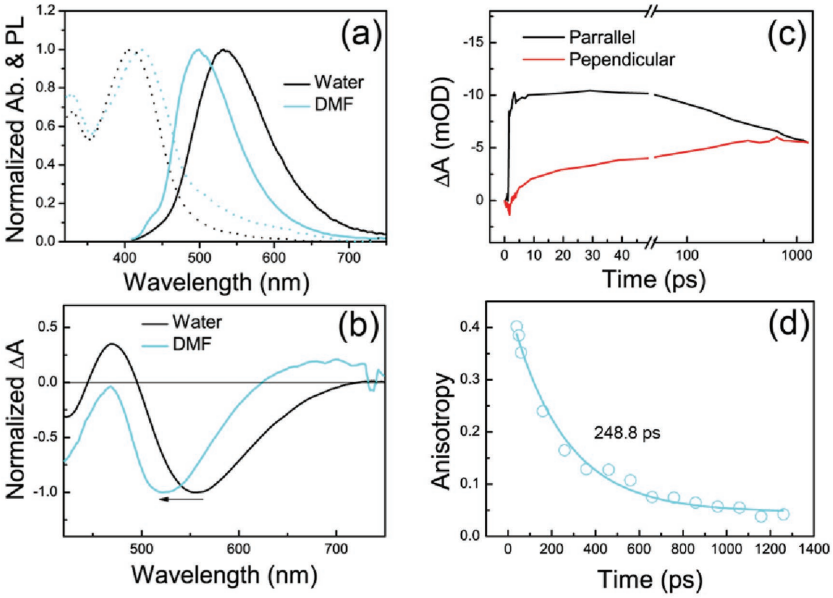

Figure 4. a) Static absorption and PL spectra and b) normalized TA spectra at delay time of 8 ps of CDots in DMF and water. c) TA kinetic traces of CDots in DMF probed at 525 nm. d) The calculated anisotropy of CDots in DMF as a function of delay time.

observed that the SE feature of CDots in DMF is blue-shifted compared to that in water (Figure 4b). The PL quantum yield (QY) of CDots in DMF enhance to 44%, which is 2.4 times higher than that in water. Additionally, the PL decay lifetime of CDots in DMF is 13.0 ns, which is significantly longer compared to that in water (5.5 ns) (Figure S10, Supporting Information). The fluorescence quenching of CDots in water could be attributed to proton transfer dynamics.[46–49] The TA kinetic traces of CDots in DMF probed at 525 nm show anisotropic stimulated emission (Figure 4c and Figure S11, Supporting Information). The depolarization time of CDots in DMF (248.8 ps) is longer than that in water (49.2 ps), even if the viscosities of DMF and water are similar (Figure 4d). The calculated hydrodynamic volume of CDots in DMF is about 1.1 nm^3 (diameter is about 1.3 nm), which is larger than that calculated in water and close to the actual size of CDots, indicating that proton transfer between protic solvent molecules and CDots could influence the depolarization process of CDots in solutions. It is inferred that PL of CDots may be related to the heteroatoms, which could act as proton accepters, such as pyridinic N and carbonyl O.

In order to well understand the anisotropic PL from CDots, we have performed the first-principles calculations based on the density functional theory (DFT). For simplicity, model 1 is monolayer graphene plate consisting of 19 aromatic rings without heteroatoms doping (**Figure 5**a). It is clearly shown that the charge density distributions of both HOMO and LUMO of model 1 are delocalized over the whole sheet, which are corresponding to π and π^* orbitals of sp^2 C domain. The energy gap between HOMO and LUMO of model 1 in our calculation is 3.54 eV (Figure 5b). In order to study the effect of pyridinic N and carbonyl O on the anisotropic PL origin of CDots, a (−N−(C=O)−N−) fragment was added at the edge of graphene plate, named as model 2. We found the charge distributions of HOMO-1 (π orbital) and LUMO (π^* orbital) are also delocalized over the whole plate. However, with heteroatoms doping, HOMO appears with the energy of 0.68 eV above HOMO-1. It can be found that the charge distribution of HOMO is mostly localized at (−N−(C=O)−N−) fragment at the edge of plate, which can be contributed from *n* electrons in doped N and O atoms.[50–52] Therefore, the dipole emission center is generated when the electron is transferred from the delocalized LUMO to the localized HOMO.

Based on the results above, we propose a possible PL mechanism, as shown in Figure 5c. HOMO of the heteroatom-doped CDots is mainly due to *n* electron of pyridinic N and carbonyl O, which is usually localized at edge of sp^2 C domain and acts as proton accepter. Proton transfer between protic solvent molecules and CDots induces PL quenching and faster depolarization process. LUMO of the CDots is related to π^* orbital of graphene-like structure, which is delocalized over sp^2 C domain. The electron in π^* orbital induces fast depolarization of ESA feature of CDots. The electron transitions between *n* orbital and π^* orbital lead to the anisotropic absorption and stimulated emission of CDots as observed in polarization-dependent TA experiment. Due to the transition dipole moments in CDots, the solvent-dependent solvation relaxation is related to the dipole–dipole interaction between CDots and polar solvent molecules.

3. Conclusion

In conclusion, we reveal the PL of heteroatom-doped CDots is originated from a kind of dipole emission centers through systematical studying solvent effect on solvation and depolarization processes by polarization-dependent femtosecond TA spectroscopy and computational simulation. Anisotropic absorption and stimulated emission were observed in different solvents, demonstrating that PL of CDot is originated from an electric dipole. Solvent effect on solvation relaxation was observed for CDots in water, ethanol, and TEG aqueous solutions, reflecting the dipole–dipole interaction between CDots and polar solvent molecules. Experimental and computational results demonstrate that the dipole emission center in CDots is relevant to electron transition between localized *n* orbital of dopant atoms (such as pyridinic N and carbonyl O) and delocalized π^* orbital of sp^2 C domain. Polarized emission is an important optical parameter for luminescent CDots, but it is still a challenge to understandi and controll their anisotropic PL. We prospect this work would provide guidance on modulating the PL properties of heteroatom-doped CDots through controlling heteroatom doping and sp^2 C conjugating domains, and promote applications of linearly polarized luminescent CDots in SPoD/ExPAN based super-resolution bioimaging, lasing materials, and polarized light-emitting diodes.

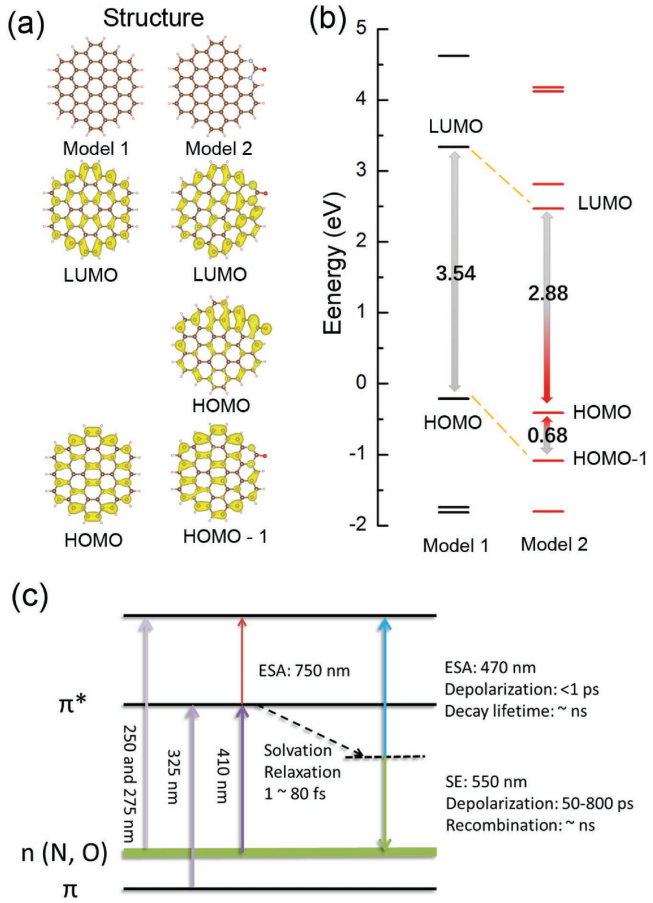

Figure 5. a) Calculated structures of model 1 and model 2. The charge distributions of LUMO, HOMO, and HOMO-1. The colored isosurface of charge density is 0.001 e Å^{-3}. b) Energy levels of model 1 and model 2. c) Model of absorption, solvation relaxation, stimulated emission, and excited state absorption processes in N and O-doped CDots.

4. Experimental Section

Synthesis and Characterization of Heteroatom-Doped CDots: Citric acid and urea were purchased from Beijing Chemical Corp. All chemicals were used as received without further purification. The water used in all experiments was purified with a Millipore system. The microwave synthesis of CDots followed procedures given in a previous work.[17] Then, the products were processed in water, followed by centrifugation (10 000 r min^{-1}, 20 min) to remove large or agglomerated particles. TEM images were recorded using a FEI-TECNAI G2 F30 transmission electron microscope operating at 200 kV. XPS spectra were recorded on an ESCALAB MK II X-ray photoelectron spectrometer. A confocal Raman microscope (Horiba Jobin Yvon, LabRAM) was used for Raman measurement with 488 nm line of an Ar^+ laser. UV–vis absorption spectra were recorded using a Shimadzu UV-3101PC spectrophotometer. Fluorescence emission spectra were recorded on a Hitachi F-7000 spectrometer. Fluorescence lifetimes were performed using Edinburgh Instruments FLS920 with 405 nm laser as the excitation source. Photoluminescence quantum yields were obtained in a calibrated integrating sphere in FLS920 spectrometer.

Transient Absorption Spectroscopy: Ultrafast TA experiments were conducted using a Ti:sapphire laser (Spectra-Physics, Spitfire ACE, 800 nm, 4.5 mJ pulse^{-1}, fwhm 35 fs, 1 kHz). Pump pulses at 400 nm were generated by frequency doubling of the fundamental laser in a BBO crystal. The white-light probe was generated by the fundamental laser output focused on a CaF_2 window. The angle between polarizations of pump and probe was changed by a $\lambda/2$ wave plate (Thorlabs, AHWP05M-340). The pump pulses were chopped by a synchronized chopper (Newport, Model 3502) to 25 Hz. After passing through the sample, the probe beam was focused into a fiber-coupled spectrometer (Ocean Optics, QE PRO). The group velocity dispersion of the whole experimental system was compensated by a chirp program. During the data collection, samples were constantly stirred to avoid degradation. All experiments were performed at room temperature.

Theoretical Calculation: The first-principles calculations based on DFT were carried out using the VASP code.[53] Projector augmented wave basis[54] and Perdew–Burke–Ernzerhof (PBE) functional[55] were employed. The cutoff energy for plane-wave basis and Monkhorst–Pack k-point mesh grid were set to 480 eV and Γ point, respectively. The pure CDot was modeled with a periodic cell of 25 Å × 15 Å × 25 Å including 54 carbon atoms and 18 hydrogen atoms, which are built in monolayer graphene sheet. The doped CDot was modeled by substituting two carbon atoms by two nitrogen atoms and adding one oxygen atom (—N—(C=O)—N—) at edge of monolayer graphene sheet, which is a simplified structure of surface group modified graphene sheet. All of atoms were relaxed until the Hellman–Feynman force is less than 0.014 eV Å^{-1}. Because the DFT calculation with PBE functional underestimates the energy gap and the energy gap has strong size-dependent effect in CDot,[56] the energy gap of CDot was shifted to the experimental value, and the level of *n* orbital in the CDot with urea fragment at the edge was shifted in proportion of the energy of *n* orbital to its HOMO versus the energy gap of CDot.

Supporting Information

Supporting Information is available from the Wiley Online Library or from the author.

Acknowledgements

This work was supported by the National Natural Science Foundation of China (Grant Nos. 51602304), Holland Research School of Molecular Chemistry (HRSMC) Fellowship program, Outstanding Young Scientists Program of Chinese Academy of Sciences, Youth Innovation Promotion Association of Chinese Academy of Sciences, and Jilin Province Science and Technology (Research Project Nos. 20150519003JH, 20160520008JH, 20170101042JC, and 20170101191JC).

Received: December 12, 2016
Revised: January 22, 2017
Published online: March 7, 2017

[1] L. Cao, X. Wang, M. J. Meziani, F. Lu, H. Wang, P. G. Luo, Y. Lin, B. A. Harruff, L. M. Veca, D. Murray, S. Y. Xie, Y. P. Sun, *J. Am. Chem. Soc.* **2007**, *129*, 11318.
[2] S. Zhu, J. Zhang, S. Tang, C. Qiao, L. Wang, H. Wang, X. Liu, B. Li, Y. Li, W. Yu, X. Wang, H. Sun, B. Yang, *Adv. Funct. Mater.* **2012**, *22*, 4732.
[3] S. T. Yang, L. Cao, P. G. Luo, F. Lu, X. Wang, H. Wang, M. J. Meziani, Y. Liu, G. Qi, Y. P. Sun, *J. Am. Chem. Soc.* **2009**, *131*, 11308.
[4] G. Leménager, E. De Luca, Y. Sun, P. P. Pompa, *Nanoscale* **2014**, *6*, 8617.
[5] A. M. Chizhik, S. Stein, M. O. Dekaliuk, C. Battle, W. Li, A. Huss, M. Platen, I. A. T. Schaap, I. Gregor, A. P. Demchenko, C. F. Schmidt, J. Enderlein, A. I. Chizhik, *Nano Lett.* **2016**, *16*, 237.
[6] L. Cao, S. Sahu, P. Anilkumar, C. E. Bunker, J. Xu, K. A. Fernando, P. Wang, E. A. Guliants, K. N. Tackett, Y. P. Sun, *J. Am. Chem. Soc.* **2011**, *133*, 4754.

[7] H. Li, X. He, Z. Kang, H. Huang, Y. Liu, J. Liu, S. Lian, C. H. Tsang, X. Yang, S. T. Lee, *Angew. Chem., Int. Ed.* **2010**, *49*, 4430.
[8] S. Zhuo, M. Shao, S. T. Lee, *ACS Nano* **2012**, *6*, 1059.
[9] M. Sun, S. Qu, W Ji, P. Jing, D. Li, L. Qin, J. Cao, H. Zhang, J. Zhao, D. Shen, *Phys. Chem. Chem. Phys.* **2015**, *17*, 7966.
[10] J. Liu, Y. Liu, N. Liu, Y. Han, X. Zhang, H. Huang, Y. Lifshitz, S. T. Lee, J. Zhong, Z. Kang, *Science* **2015**, *347*, 970.
[11] V. Gupta, N. Chaudhary, R. Srivastava, G. D. Sharma, R. Bhardwaj, S. Chand, *J. Am. Chem. Soc.* **2011**, *133*, 9960.
[12] Y. Li, Y. Hu, Y. Zhao, G. Shi, L. Deng, Y. Hou, L. Qu, *Adv. Mater.* **2011**, *23*, 776.
[13] X. Yan, X. Cui, B. Li, L. S. Li, *Nano Lett.* **2010**, *10*, 1869.
[14] X. Zhang, Y. Zhang, Y. Wang, S. Kalytchuk, S. V. Kershaw, Y Wang, P. Wang, T. Zhang, Y. Zhao, H. Zhang, T. Cui, Y. Wang, J. Zhao, W. W. Yu, A. L. Rogach, *ACS Nano* **2013**, *7*, 11234.
[15] W. Kwon, Y. H. Kim, C. L. Lee, M. Lee, H. C. Choi, T. W. Lee, S. W. Rhee, *Nano Lett.* **2014**, *14*, 1306.
[16] W. F. Zhang, H. Zhu, S. F. Yu, H. Y. Yang, *Adv. Mater.* **2012**, *24*, 2263.
[17] S. Qu, X. Liu, X. Guo, M. Chu, L. Zhang, D. Shen, *Adv. Funct. Mater.* **2014**, *24*, 2689.
[18] V. Georgakilas, J. A. Perman, J. Tucek, R. Zboril, *Chem. Rev.* **2015**, *115*, 4744.
[19] Y. P. Sun, B. Zhou, Y. Lin, W. Wang, K. A. S. Fernando, P. Pathak, M. J. Meziani, B. A. Harruff, X. Wang, H. F. Wang, P. J. G. Luo, H. Yang, M. E. Kose, B. L. Chen, L. M. Veca, S. Y. Xie, *J. Am. Chem. Soc.* **2006**, *128*, 7756.
[20] S. N. Baker, G. A. Baker, *Angew. Chem., Int. Ed.* **2010**, *49*, 6726.
[21] S. Qu, X. Wang, Q. Lu, X. Liu, L. Wang, *Angew. Chem., Int. Ed.* **2012**, *51*, 12215.
[22] K. Hola, Y. Zhang, Y. Wang, E. P. Giannelis, R. Zboril, A. L. Rogach, *Nano Today* **2014**, *9*, 590.
[23] V. Strauss, J. T. Margraf, K. Dirian, Z. Syrgiannis, M. Prato, C. Wessendorf, A. Hirsch, T. Clark, D. M. Guldi, *Angew. Chem., Int. Ed.* **2015**, *54*, 8292.
[24] S. Ghosh, A. M. Chizhik, N. Karedla, M. O. Dekaliuk, I. Gregor, H. Schuhmann, M. Seibt, K. Bodensiek, I. A. T. Schaap, O. Schulz, A. P. Demchenko, J. Enderlein, A. I. Chizhik, *Nano Lett.* **2014**, *14*, 5656.
[25] A. I. Chizhik, A. M. Chizhik, D. Khoptyar, S. Bär, A. J. Meixner, *Nano Lett.* **2011**, *11*, 1131.
[26] J. Hu, L. S. Li, W. Yang, L. Manna, L. W. Wang, A. P. Alivisatos, *Science* **2001**, *292*, 2060.
[27] P. D. Cunningham, J. E. Boercker, D. Placencia, J. G. Tischler, *ACS Nano* **2014**, *8*, 581.
[28] N. Hafi, M. Grunwald, L. S. van den Heuvel, T. Aspelmeier, J. H. Chen, M. Zagrebelsky, O. M. Schütte, C. Steinem, M. Korte, A. Munk, P. J. Walla, *Nat. Methods* **2014**, *11*, 579.
[29] D. Qu, M. Zheng, J. Li, Z. G. Xie, Z. C. Sun, *Light: Sci. Appl.* **2015**, *4*, e364.
[30] D. Qu, Z. C. Sun, M. Zheng, J. Li, Y. Q. Zhang, G. Q. Zhang, H. F. Zhao, X. Y. Liu, Z. G. Xie, *Adv. Opt. Mater.* **2015**, *3*, 360.
[31] F. Arcudi, L. Đorđević, M. Prato, *Angew. Chem., Int. Ed.* **2016**, *55*, 2107.
[32] X. M. Wen, P. Yu, Y. R. Toh, X. T. Hao, J. Tang, *Adv. Opt. Mater.* **2013**, *1*, 173.
[33] L. Wang, S. J. Zhu, H. Y. Wang, Y. F. Wang, Y. W. Hao, J. H. Zhang, Q. D. Chen, Y. L. Zhang, W. Han, B. Yang, H. B. Sun, *Adv. Opt. Mater.* **2013**, *1*, 264.
[34] L. Wang, S. J. Zhu, H. Y. Wang, S. Qu, Y. L. Zhang, J. H. Zhang, Q. D. Chen, H. Xu, W. Han, B. Yang, H. B. Sun, *ACS Nano* **2014**, *8*, 2541.
[35] A. Sharma, T. Gadly, A. Gupta, A. Ballal, S. K. Ghosh, M. Kumbhakar, *J. Phys. Chem. Lett.* **2016**, *7*, 3695.
[36] S. Khan, A. Gupta, N. C. Verma, C. K. Nandi, *Nano Lett.* **2015**, *15*, 8300.
[37] N. Dhenadhayalan, K. C. Lin, R. Suresh, P. Ramamurthy, *J. Phys. Chem. C* **2016**, *120*, 1252.
[38] M. O. Dekaliuk, O. Viagin, Y. V. Malyukin, A. P. Demchenko, *Phys. Chem. Chem. Phys.* **2014**, *16*, 16075.
[39] M. Glasbeek, H. Zhang, *Chem. Rev.* **2004**, *104*, 1929.
[40] J. R. Lakowicz, Topics in Fluorescence Spectroscopy, *Nonlinear and Two-Photon-Induced Fluorescence*, Vol. *5*, Kluwer Academic, New York **2002**.
[41] R. Jimenez, G. R. Fleming, P. V. Kumar, M. Maroncelll, *Nature* **1994**, *369*, 471.
[42] W. Jarzqba, G. C. Walker, A. E. Johnson, M. A. Kahlow, P. F. Barbara, *J. Phys. Chem.* **1988**, *92*, 7039.
[43] M. Mittendorff, T. Winzer, E. Malic, A. Knorr, C. Berger, W. A. de Heer, H. Schneider, M. Helm, S. Winnerl, *Nano Lett.* **2014**, *14*, 1504.
[44] J. R. Lakowicz, *Principles of Fluorescence Spectroscopy*, 3rd ed., Springer, Berlin, Germany **2006**.
[45] C. C. Hsieh, C. M. Jiang, P. T. Chow, *Acc. Chem. Res.* **2010**, *43*, 1364.
[46] H. T. Yu, W. J. Colucci, M. L. McLaughlin, M. D. Barkley, *J. Am. Chem. Soc.* **1992**, *114*, 8449.
[47] G. J. Zhao, K. L. Han, *Acc. Chem. Res.* **2012**, *45*, 404.
[48] A. Sciortino, E. Marino, B. van Dam, P. Schall, M. Cannas, F. Messina, *J. Phys. Chem. Lett.* **2016**, *7*, 3419.
[49] L. Sui, W. Jin, S. Li, D. Liu, Y. Jiang, A. Chen, H. Liu, Y. Shi, D. Ding, M. Jin, *Phys. Chem. Chem. Phys.* **2016**, *18*, 3838.
[50] M. Sudolská, M. Dubecký, S. Sarkar, C. J. Reckmeier, R. Zbořil, A. L. Rogach, M. Otyepka, *J. Phys. Chem. C* **2015**, *119*, 13369.
[51] S. Sarkar, M. Sudolská, M. Dubecký, C. J. Reckmeier, A. L. Rogach, R. Zbořil, M. Otyepka, *J. Phys. Chem. C* **2016**, *120*, 1303.
[52] W. Kwon, S. Do, J. H. Kim, M. S. Jeong, S. W. Rhee, *Sci. Rep.* **2015**, *5*, 12604.
[53] G. Kresse, J. Furthmüller, *Comput. Mater. Sci.* **1996**, *6*, 15.
[54] P. E. Blochl, *Phys. Rev. B* **1994**, *50*, 17953.
[55] J. P. Perdew, K. Burke, M. Ernzerhof, *Phys. Rev. Lett.* **1996**, *77*, 3865.
[56] G. Eda, Y. Y. Lin, C. Mattevi, H. Yamaguchi, H. A. Chen, I. S. Chen, C. W. Chen, M. Chhowalla, *Adv. Mater.* **2010**, *22*, 505.